Energy 316 (2025) 134517

Contents lists available at ScienceDirect

Energy

journal homepage: www.elsevier.com/locate/energy

An environmentally sustainable energy management strategy for marine hybrid propulsion

Luca Maloberti *, Raphael Zaccone

Department of Electrical, Electronics, Telecommunication Engineering and Naval Architecture (DITEN), Polytechnic School, University of Genoa, Via Montallegro 1, Genoa, 16145, Italy

ARTICLE INFO

Keywords:
Marine hybrid propulsion
Energy management
Optimization
Energy storage system
Fuel-cell
Hydrogen

ABSTRACT

Integrating electric technologies, such as battery energy storage systems and electric propulsion, has become an appealing option for reducing fuel consumption and emissions in the transportation sector, making these technologies increasingly popular for research and industrial application in the maritime sector. In addition, hydrogen is a promising technology for reducing emissions, although hydrogen production technologies significantly influence the overall impact of hydrogen-powered systems. This paper proposes an optimization-based strategy to minimize the environmental impact of a hybrid propulsion system over a given load profile, while furthermore considering the environmental impact resulting from the hydrogen production chain. The propulsion system includes diesel generators, hydrogen-powered fuel cells, batteries, and electric motors; mathematical models and assumptions are discussed in detail.

The paper applies the proposed strategy, and compares different hybrid solutions considering equivalent CO_2 emissions, discussing a test case applied to a short-range ferry operating in a marine protected area, an area particularly sensitive to the problem of atmospheric emissions. The results demonstrate that the proposed strategy can reduce greenhouse gas emissions by up to 73% compared to a conventional mechanical propulsion system.

1. Introduction

Over the past 40 years, maritime transport has undergone a remarkable transformation, registering a substantial increase of 250%. This growth rate has outpaced world population growth (90%) and energy consumption growth (170%), aligning with the expansion of the world's gross domestic product [1]. This significant surge in shipping highlights its growing importance in global trade and its integral role in connecting economies worldwide.

Shipping is responsible for approximately 3% of the overall yearly emissions of human-made Greenhouse gas (GHG), particularly Carbon Dioxide (CO_2) [2]. If current trends continue, emissions will surge by 150%–250% within 2050, while global trade will triplicate. In contrast, the European Union has established a goal of achieving net zero CO_2 emissions by 2050 to limit global temperature rise to 1.5 °C.

Compared to other modes of transportation, such as air and road, maritime transport stands out for its significant energy efficiency because of two key factors: the large carrying capacity of ships and the lower fuel consumption per ton of cargo transported [1]. Maritime transport offers a more sustainable transportation option by leveraging economies of scale and optimizing payload, reducing energy consumption and carbon emissions. This approach helps minimize the environmental impact and makes maritime transport a more eco-friendly choice for transportation.

Moreover, maritime transport is vital to global trade, accounting for 90% of world trade freight. This dominance position makes the marine sector a crucial contributor to achieving sustainability targets in the transportation sector [3]. Even minor improvements in energy efficiency, operational practices, and emissions reduction within maritime transport can yield substantial environmental benefits. With its immense scale and reach, maritime transport presents a unique opportunity to make significant footsteps toward a more sustainable future. By embracing innovative technologies, adopting cleaner fuels, and implementing effective policies and regulations, the maritime industry has the potential to enhance its energy efficiency further and reduce its environmental impact. Collaborative efforts between governments, international organizations, and the shipping industry are crucial in driving these improvements and ensuring that maritime transport facilitates global trade while minimizing its carbon footprint.

Due to the increasing attention to the environment and the enforcement of increasingly strict emission regulations by the International

* Corresponding author.
E-mail addresses: luca.maloberti@edu.unige.it (L. Maloberti), raphael.zaccone@unige.it (R. Zaccone).

https://doi.org/10.1016/j.energy.2025.134517
Received 24 August 2023; Received in revised form 11 January 2025; Accepted 11 January 2025
Available online 20 January 2025

Abbreviations

$B56$	"Blue" hydrogen with $56\%CCS$
$B90$	"Blue" hydrogen with $90\%CCS$
$BESS$	Battery Energy Storage System
$BSEC$	Brake-Specific Energy Consumption
$BSPC$	Brake-Specific Pilot Consumption
$BSXC$	Brake-Specific Consumption of the generic fuel X
CCS	Carbon Capture and Storage
DG	Diesel Generator
EF	Emission Factor
FC	Fuel Cell
G	"Green" hydrogen produced by $PEMEL$ from Italian production toolchain
$G+$	"Green" hydrogen produced by $PEMEL$ from Norwegian production toolchain
GHG	Greenhouse gas
GWP	Global Warming Potential
K	"Gray" hydrogen produced by SMR
LHV	Lower Heating Value
MP	Methane Pyrolysis
$PEMEL$	Polymer Electrolyte Membrane Electrolysis
$SFOC$	Specific Fuel Oil Consumption
SMR	Steam Methane Reforming
SoC	State-of-Charge
T	"Turquoise" hydrogen produced by MP

Maritime Organization [4], a profound transformation is underway within the maritime industry's approach. This shift is particularly evident in the propulsion system design field, where there is a growing demand for solutions that are not only technologically advanced but also environmentally sustainable [5–7].

In the context of small-sized vessels that primarily operate over short distances, such as in coastal areas or inland waterways, previous results suggested that zero-emission propulsion systems employing lithium-ion batteries recharged via the on-shore power grid can help reduce the environmental impact [8]. This approach holds promise for significantly reducing emissions in these specific contexts. However, this solution may not be viable for larger ships with long-range requirements due to the weight of currently available batteries and the technological limits of the on-shore infrastructure. Consequently, the maritime industry and the research community actively explore alternatives and opportunities to reduce pollutant emissions and enhance energy efficiency, such as low-emission fuels, (Liquefied Natural Gas, Methanol, Ammonia, Bio-Fuel, and E-Fuel), or on-board power generation technologies, including Fuel-cells and Photovoltaic panels [1,9–11]. These technologies offer potential alternatives to traditional Diesel Engines and can be integrated into hybrid configurations along with conventional propulsion systems [12].

Hybridization, in particular, might provide fuel savings ranging from 10% to 40% and remarkably short payback periods, some as low as one year [13]. Moreover, adopting hybrid propulsion enables greater flexibility in vessel design, allowing ship operators to accommodate financial and environmental requirements [14–16].

Hybrid marine propulsion systems offer versatile options to match requirements such as ship type, component sizing, system layout, and desired performance. Energy storage devices such as Battery Energy Storage System ($BESS$) can provide several benefits to ship safety and operation: Firstly, $BESS$ can operate as uninterruptable power supplies to prevent blackouts and enhance safety. Moreover, $BESS$ can operate as a power reserve to shave the power demand peaks and improve the dynamic performance of the propulsion system, allowing gradual generator loading and unloading. Eventually, $BESS$ can significantly improve energy efficiency and reduce environmental impact, allowing the diesel generators' strategic loading and zero-emission operation for a limited time.

Hydrogen is gaining interest as an efficient energy carrier [17] as an alternative to conventional fuels, particularly as a reactant in fuel cells in combination with other technologies to improve the sustainability of power systems [18]. However, the sustainability of hydrogen production presents some major challenges. Despite being the most abundant chemical element in the atmosphere, it does not exist in pure molecular form and must be extracted from other substances, including natural gas, oil, coal, or water. Hydrogen can be categorized into four types based on the production method: "gray" hydrogen is obtained by Steam Methane Reforming (SMR), "blue" hydrogen is produced through SMR but with Carbon Capture and Storage (CCS), "turquoise" is obtained by methane pyrolysis, "green" is produced using the electrolysis of water [19]. If the production relies on clean energy sources like solar, wind, or geothermal power, using "green" hydrogen features neglectable emission of pollutants over the complete toolchain. On the other hand, if the electric energy used in the production comes from traditional sources, "green" hydrogen provides limited environmental benefits.

The main advantage of hybrid systems is the ability to use different technologies by exploiting the advantage of each and compensating for the limitations. In complex hybrid systems, however, the best technology to exploit to fulfill the power demand may not be evident, especially if the ship has a varied operating profile characterized by different power and speed requirements. In this case, numerical optimization provides practical help. Some optimization-based approaches to hybrid systems are described in the literature, based on stationary modeling of the different components of the system and solving them using appropriate algorithms. Zaccone et al. [20] presented an optimization-based design of diesel-electric propulsion systems minimizing consumption, using a genetic algorithm to determine the number, type, and power of engines installed on board, selecting from within a dataset of four-stroke diesel engines. The optimal load-sharing strategy under off-design conditions is also determined using the same algorithm. This approach is then applied to a case study, and AC and DC grid solutions are compared and discussed under design and off-design conditions. D'Agostino et al. [21] used Mixed Integer Linear Programming techniques to determine the optimal utilization strategy for a hybrid plant with diesel generators and $BESS$, minimizing the economic cost of fuel, by validating the simulation on an electrical load modeled starting from real measurements. Al-Falahi et al. [22] presented a minimum fuel consumption-oriented optimization approach based on the grey-wolf optimization algorithm applied to a hybrid system with batteries and diesel generators and compared the results to a rule-based power management strategy. Kanellos [23] proposed a method for optimal energy management and greenhouse gas emission reduction for all-electric ships, optimizing the power generation and speed based on a shipload forecast using dynamic programming combined with a stochastic evolutionary optimization method. Gallo et al. [24] proposed a methodology to estimate the environmental performance of a ship during the preliminary design phase based on mission analysis, simulating different power plant configurations, including diesel generators with different fuels, battery energy storage systems, fuel cells and hydrogen storage systems. Different rule-based energy management strategies are tested to exploit various resources while maximizing the requirements of operating conditions. The configurations considered are compared based on different performance indicators to identify the preliminary design solution.

This paper proposes an optimization strategy to determine the optimal power split to minimize the environmental impact of a hybrid marine propulsion system featuring a diesel generator set, a $BESS$, and hydrogen-powered fuel cells. The optimization aims to minimize the

equivalent CO_2 produced by the system during the mission. First, the paper defines and discusses the models of the system components, such as diesel generators, $BESS$, and fuel cells. Next, the formulation of a constrained optimum problem is proposed, the solution of which yields the best strategy for using the different components during the vessel's mission to minimize emissions. The presented strategy is applied to a case study of a passenger ferry operating in the marine protected area "Cinque Terre" on Italy's northwest coast, between La Spezia and Levanto ports. The typical daily mission profile features high speed cruising to reduce the overall travel time, and low-speed cruising inside the protected area. Hybrid propulsion systems are highly flexible and allow finding a meeting point between the different requirements. The mission is defined in detail by deriving the power demand profile. The paper compares the optimal utilization of different system configurations characterized by component combinations and hydrogen production technologies.

2. Power system modeling

The proposed modeling approach focuses on achieving a homogeneous level of approximation among the models. Static lumped-element models have been used to estimate proper quantities useful to compare different propulsive solutions. The overall goal of the models presented is to represent the performance of the systems modeled in order to estimate the effects that an operational choice such as power-splitting among available machinery can have on overall plant performance relative to a mission profile. This section discusses the mathematical modeling of the power system components: the heat engines, the $BESS$, and the fuel cells.

2.1. Heat engines

Various mathematical models in existing literature rely on different approximation levels [25]. Within this study, the heat engines are modeled using Brake-Specific Energy Consumption (BSEC) to represent the fuel mass flow rate as a function of the power output [26]:

$$\dot{m}_{fuel} = \frac{P_B\ BSEC}{LHV_{fuel}} \tag{1}$$

where P_B is the brake power, LHV is the lower heating value, and the $BSEC$ is a function of the brake power and the engine speed. Such an approach is simplified and flexible enough to describe different fuels, such as fuel oil, natural gas, ammonia, or methanol [24]. The engine model for a generic fuel and diesel pilot injection is obtained by considering the Brake-Specific Consumption of the generic fuel X ($BSXC$) and the Brake-Specific Pilot Consumption ($BSPC$):

$$\begin{cases} \dot{m}_X = \dfrac{P_B\ BSXC}{LHV_X} \\ \dot{m}_{pilot} = \dfrac{P_B\ BSPC}{LHV_{pilot}} \end{cases} \tag{2}$$

where X and $pilot$ subscripts indicate the generic fuel X and the pilot fuel oil, respectively. For a Diesel engine, specific fuel oil consumption ($SFOC$) is often used in place of $BSEC$:

$$SFOC = \frac{BSEC}{LHV} \tag{3}$$

The fuel mass flow rate is determined as follows:

$$\dot{m}_{fuel} = P_B\ SFOC \tag{4}$$

In principle, $SFOC$ is a function of the power output of the engine and its speed. Since the speed of diesel generators is usually controlled, the speed can be considered a function of power, and consequently, the explicit dependence is neglected. To this end, $SFOC$ is modeled as a 2nd order polynomial function of the engine power output [27]:

$$SFOC = a\left(\frac{P_B}{P_{MCR}}\right)^2 + b\frac{P_B}{P_{MCR}} + c \tag{5}$$

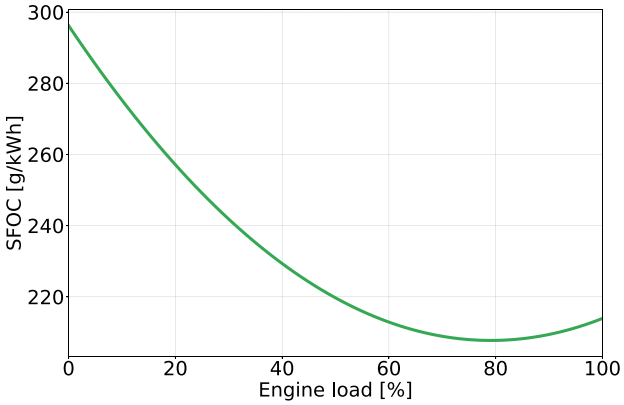

Fig. 1. Specific fuel oil consumption curve.

where P_{MCR} is the engine's rated power, a, b, and c can be estimated to fit the engine manufacturer's data. Fig. 1 shows the $SFOC$ curve used in this study, considering Marine Diesel Oil (MDO) as fuel. Notice that the optimal operating range for the considered diesel engine falls between 70% and 90% of its rated power.

2.2. Battery energy storage system

A $BESS$ is an energy storage device whose voltage depends on the current and the battery energy content. There is a wide variety of approaches to battery modeling in scientific literature [28]. A widely adopted approach to describe a battery is Sheperd's model Zaccone et al. [29], expressing the voltage $V(t)$ as a function of the current $i(t)$:

$$V(t) = V_0 - Ri(t) - k\frac{Q_{max}}{Q_{max} - \int_0^t i(\tau)d\tau} + Ae^{-B\int_0^t i(\tau)d\tau} \tag{6}$$

where V_0 is the constant voltage component, R is the internal resistance of the battery, k is the polarization voltage, Q_{max} is the battery capacity, A is the amplitude of the exponential zone, and B is the inverse of the exponential time constant. The battery state of charge (SoC) is defined as follows:

$$SoC(t) = \frac{Q_0 - \int_0^t i(\tau)d\tau}{Q_{max}} \tag{7}$$

where Q_0 is the charge at time $t = 0$.

For technological reasons, the SoC should be kept within its central range, usually between 30% and 85%. In this range, polarization and exponential terms can be neglected. The battery efficiency η_{BESS} can be defined as:

$$\eta_{BESS} = \frac{E_0 - E_{loss}}{E_0} \tag{8}$$

where E_{loss} is the energy loss due to the voltage drop ΔV during the charge–discharge process. Neglecting the polarization and exponential terms in Eq. (6), the battery efficiency takes the following form:

$$\eta_{BESS} = 1 - \frac{2Ri(t)}{V_0} \tag{9}$$

The SoC can then be calculated by re-writing Eq. (7) in terms of energy and considering the battery efficiency defined in Eq. (8), according to the following equation:

$$\begin{cases} SoC(t) = SoC(0) - \dfrac{\beta}{E_{BESS}}\displaystyle\int_0^T P_{BESS}(t)dt \\ \beta = \begin{cases} 1 & \text{if } P_{BESS} \le 0 \\ \eta_{BESS} & \text{if } P_{BESS} > 0 \end{cases} \end{cases} \tag{10}$$

where $SoC(0)$ is SoC at time $t = 0$, η_{BESS} is the battery efficiency, P_{BESS} is the power delivered by the $BESS$, which can be positive or negative, depending on whether we are in the charging or discharging phase, and E_{BESS} is the nominal energy stored in the battery.

2.3. Fuel cell

A fuel cell is an electrochemical device generating an electric potential by facilitating the reaction between hydrogen and oxygen:

$$H_2 + \frac{1}{2}O_2 \rightarrow H_2O \tag{11}$$

Fuel cells share some characteristics with batteries, such as their modular structure and reliance on electrochemical reactions. However, the main distinction lies in the fuel cell's use of externally introduced reactants and the disposal of the reaction products. Several approaches to fuel cell modeling exist in the literature, some parametric-empirical, others based on electrochemical models. The formers are the most appropriate starting point for the present work and are based on the partitioning of the potential at the cell terminals [30–32] according to the following equation:

$$V_{cell} = V_{rev} - V_{act} - V_{ohm} - V_{conc} \tag{12}$$

where V_{cell} is the potential at the cell's terminals, V_{rev} is the reversible potential. The sum of potentials V_{act}, V_{ohm}, V_{conc}, activation, ohmic, and concentration potentials, respectively, is the so-called irreversible potential. The reversible potential is usually described through the Nernst Equation, which allows the standard reaction potential to be corrected for the effect of temperature and the partial pressures partial of the species involved in the reaction (hydrogen, oxygen, and water). This paper neglects the impact of temperature and gas partial pressures and the activation and concentration losses. The fuel cell is thus modeled through a resistive-only equivalent circuit. The electrical power delivered by a stack of N cells in series is calculated according to the following equation:

$$P_{FC}(t) = NV_0 i(t) - NRi^2(t) = V_{FC} i(t) - R_{FC} i^2(t) \tag{13}$$

where V_0 is the cell open circuit potential, R is the internal resistance, i is the current, and FC subscript refers to the whole cell stack. The following equation gives the reactant flow rate of the stack [33]:

$$\begin{cases} \dot{m}_{H_2}(t) = \dfrac{M_{H_2} N}{2F} i(t) \\ \dot{m}_{O_2}(t) = \dfrac{M_{O_2} N}{4F} i(t) \end{cases} \tag{14}$$

where M_{H_2} and M_{O_2} are the reactant molar masses and F is the Faraday constant. Combining Eqs. (13) and (14), and solving the resulting 2nd order equation for $\dot{m}_{H_2}$, the expression of the hydrogen flow rate of the stack as a function of the fuel cell power is obtained:

$$\dot{m}_{H_2}(t) = \frac{M_{H_2} N}{2F} \left[\frac{V_{FC} - \sqrt{V_{FC}^2 - 4R_{FC} P_{FC}(t)}}{2R_{FC}} \right] \tag{15}$$

3. Performance indicators

The performance indicators presented in this section aim at measuring the energy efficiency and environmental impact of a power system and are used to evaluate the cost function of the optimization problem and to compare the performance of different propulsion configurations. To this end, performance indicators include the system's fuel consumption and the equivalent CO_2 production. Particular attention is given to the evaluation of the pollutant emission of the hydrogen production toolchain.

3.1. Fuel consumption and pollutant emissions

Fuel consumption can be used as a performance indicator to assess the energy efficiency of a power system. Lower fuel consumption identifies higher efficiency for the same amount of expended energy. The total mass of burned fuel m_{fuel} is evaluated according to the following equation:

$$m_f = \int_0^T \dot{m}_f(\tau) d\tau \tag{16}$$

where $\dot{m}_f$ is the fuel mass flow rate obtained through Eq. (4). The mass of pollutant gas produced by fuel combustion can be evaluated using the emission factors. In particular, the mass of the generic pollutant X m_X is computed according to the following equation:

$$m_X = EF_X \, m_{fuel} \tag{17}$$

where EF_X is the emission factor, expressing the mass of pollutant X per mass unit of fuel. Table 1 shows the emission factors (GHG) of the main Greenhouse Gases produced by the combustion of Marine Diesel Oil [34].

Table 1
Global warming potential and emission factor for different GHG produced by the combustion of MDO.

GHG	EF [kg/t_{MDO}]	GWP
Carbon dioxide (CO_2)	3140	1
Methane (CH_4)	0.18	21
Nitrous oxide (N_2O)	1.3	310
Equivalent CO_2 ($CO_{2\,eq}$)	3547	

3.2. Equivalent CO_2

The reference standards consider (CO_2) emissions to quantify the global warming impact of a process, neglecting the other GHG. To fully assess the environmental impact of a technological solution, equivalent CO_2 ($CO_{2\,eq}$) integrates the contribution of the different GHG to global warming by converting them to the equivalent amount of carbon dioxide with the same global warming potential [8].

Each greenhouse gas, e.g., carbon dioxide (CO_2), methane (CH_4), and nitrous oxide (N_2O), has a Global Warming Potential (GWP), is a measure of how much infrared thermal radiation a greenhouse gas added to the atmosphere would absorb over a 100-year time frame, as a multiple of the radiation that would be absorbed by the same mass of added CO_2 [35]. Table 1 presents the GWP of the main GHG [36].

The mass of equivalent CO_2 $m_{CO_{2\,eq}}$ is the sum of the emissions of all greenhouse gases, weighted by their Global Warming Potential according to the following equation:

$$m_{CO_{2\,eq}} = \sum_i m_i \, GWP_i \tag{18}$$

where m_i is the mass of the ith GHG, computed according to Eq. (18), and GWP_i is its global warming potential. By combining the GWP of GHG and their emission factors (Table 1), the emission factor of equivalent CO_2 can be calculated:

$$EF_{CO_{2\,eq}} = \sum_i GWP_i \, EF_i \tag{19}$$

where i represent the ith GHG.

The waste product of the reactions inside the fuel cell is water, making this technology intrinsically zero-emission, at least locally. However, the emissions of the hydrogen production toolchain can be assessed via proper emission factors [19] depending on the production technology. The emission factors used to account for the different production technologies are shown in Table 2. The production technologies range from Steam Methane Reforming (SMR) without or with carbon capture and storage (CCS), Methane Pyrolysis (MP), and Polymer Electrolyte Membrane Electrolysis ($PEMEL$). Table 2 refers to Italy to be consistent with the proposed case study. Since the Italian production of "green" hydrogen primarily relies on nonrenewable sources, "green" hydrogen is the worst solution in terms of environmental impact. The Norwegian emission factor is reported to give a perspective of the best-case scenario.

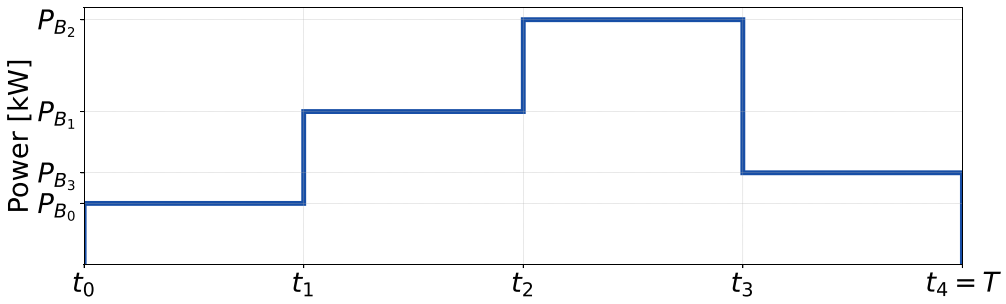

Fig. 2. Example of a load profile.

Table 2
Emission factors of hydrogen production (Italy).

Short name	Technology	EF [kg/kg]
Gray	SMR	11.7
Blue	$SMR-CCS$ (56%)	7.4
Blue	$SMR-CCS$ (90%)	4.6
Turquoise	MP	7.5
Green	$PEMEL$	20.4
Green (Norway)	$PEMEL$	0.8

4. Methodology

The presented strategy aims at computing the optimal use of power sources to minimize equivalent CO_2 emissions for a given mission profile, i.e., the optimal power split to fulfill the power request. This section describes the problem formulation, including the constraints, cost function, and solving algorithm.

4.1. Parametrization

Fig. 2 provides a qualitative representation of an example input load profile. The mission is defined at discrete time instants t_j, $j = 0 \dots T$ corresponding to the variations of the required power. Every step represent a shift in power demand P_j the system has to meet at each discrete time instant. The variables identifying the optimal solution are the power outputs of the diesel generators and the fuel cell, expressed as a fraction of the respective maximum power through proper load coefficient α. The variables at time t_j can be summarized into a vector X_j:

$$X_j = \left\{ \alpha^j_{DG_1}, \alpha^j_{DG_2}, \dots \alpha^j_{DG_n} \alpha^j_{FC} \right\} \tag{20}$$

where $\alpha^j_{DG_i}$ and α^j_{FC} are the load coefficients of the ith Diesel Generator (DG) and the Fuel Cell (FC) at time t_j, respectively, n is the number of DG installed on-board. A candidate solution takes the following form:

$$\mathbf{X} = \left\{ X_j \right\}, \; j = 0 \dots (T-1) \tag{21}$$

The power delivered by generators and fuel cell at each time-instant t_j is calculated according to the following equation:

$$P^j_m = \alpha^j_m \, P^{max}_m \tag{22}$$

where the subscript m represents the DG and the FC. The battery power is calculated as the difference between the load and the power delivered by the other components.

4.2. Constraints

The following subsection discusses the problem's constraints: the bounds, the power balance constraint, and the component-specific constraints.

The power generated from each generator and the fuel cell must be within the respective allowable ranges:

$$\begin{cases} 0 \le \alpha^j_{DG_i} P^{max}_i \le P^{max}_i \\ 0 \le \alpha^j_{FC} P^{max}_{FC} \le P^{max}_{FC} \end{cases} \tag{23}$$

where $P^{max}_{DG_i}$ and P^{max}_{FC} are the maximum power generated by the ith DG and the fuel cell, respectively, and $\alpha^j_{DG_i}$ and α^j_{FC} are the respective load coefficients.

The power that charges or discharges the $BESS$ is obtained as the difference between the power generated and the power required by the load. This power cannot exceed the maximum power limits of the $BESS$. The power balance constraint, therefore, takes the following form:

$$-P^{max,c}_{BESS} \le P_{FC_j} + \sum_{i=1}^{n} P_{i,j} - P_{load_j} \le P^{max,d}_{BESS} \tag{24}$$

where P_i is the power delivered by the ith generator, P_{FC} is the power delivered by the Fuel Cell, P_{BESS} is the $BESS$ power, P_{load} is the power demand, and $P^{max,d}_{BESS}$, $P^{max,c}_{BESS}$ are the maximum power in discharge and charge, respectively.

Moreover, two Battery Storage System constraints need to be set. Firstly, the SoC of the $BESS$ is limited between a minimum (SoC^{min}) and maximum (SoC^{max}) to preserve the battery state of health:

$$SoC^{min} \le SoC_j \le SoC^{max} \tag{25}$$

The SoC_j at time t_j obtained by discretizing Eq. (10), is given by:

$$SoC_j = \frac{1}{E_{max}} \left(E_0 - \beta \sum_{p=0}^{j} P_{BESS_p} \Delta t_p \right) \tag{26}$$

where $\Delta t_p = t_p - t_{p-1}$.

Secondly, the battery energy balance constraint is required to keep the results consistent:

$$SoC_0 = SoC_T \tag{27}$$

Eventually, consumption must not exceed the hydrogen available on board:

$$m_{\mathrm{H}_2} = \sum_{j=0}^{T} \dot{m}_{\mathrm{H}_2}(\alpha^j_{FC}) \Delta t_j \le \mathrm{H}^{on-board}_2 \tag{28}$$

where $\mathrm{H}^{on-board}_2$ is the total mass of hydrogen on-board, $\Delta t_j = t_{j+1} - t_j$, and $\dot{m}_{\mathrm{H}_2}$ is the hydrogen flow rate, which is a function of the fuel cell load coefficient and is calculated by substituting Eq. (22) in Eq. (15):

$$\dot{m}_{\mathrm{H}_2 j} = \frac{M_{\mathrm{H}_2} N}{2F} \left[\frac{V_{FC} - \sqrt{V^2_{FC} - 4R_{FC} \left(\alpha^j_{FC} P^{max}_{FC} \right)}}{2R_{FC}} \right] \tag{29}$$

4.3. Loss function

Since the primary objective is to minimize the environmental impact, the equivalent CO_2 emissions ($CO^{tot}_{2\,eq}$), representing the loss function of the optimization problem, is minimized throughout the ship's mission:

$$CO^{tot}_{2\,eq} = CO^{DGs}_{2\,eq} + CO^{H_2}_{2\,eq} \tag{30}$$

The $CO_{2\,eq}$ emitted by the DG ($CO^{DGs}_{2\,eq}$) is calculated according to the following equation:

$$CO^{DGs}_{2\,eq} = EF_{fuel} \sum_{j=0}^{T} \sum_{i=1}^{n} \alpha^{j}_{DG_i} P^{max}_{i} SFOC_i(\alpha^{j}_{DG_i}) \Delta t_j \tag{31}$$

where EF_{fuel} is the equivalent CO_2 emission factor for the MDO, $\alpha^{j}_{DG_i}$ is the load coefficient of the ith DG at time jth, P^{max}_{i} is its maximum power, and $SFOC_{i,j}$ is the specific fuel oil consumption of the ith DG at the jth time. The amount of equivalent CO_2 associated with hydrogen consumption is evaluated according to the following equation, depending on the hydrogen production technology:

$$CO^{H_2}_{2\,eq} = EF_{H_2} \sum_{j=0}^{T} \dot{m}_{H_{2_j}} (\alpha^{j}_{FC}) \Delta t_j \tag{32}$$

where EF_{H_2} is the equivalent CO_2 emission factor and $\dot{m}_{H_2}$ is the hydrogen mass flow rate for each time instant j defined in Eq. (29).

4.4. Problem setup and solution

The following optimization problem combines Eqs. (24), (25), (27), (28), (23) and (31) needs to be solved to determine the optimal management of the on-board energy sources:

$$\begin{cases} \min\limits_{\mathbf{X}} \; CO^{tot}_{2\,eq}(\mathbf{X}) \\ s.t. : \\ 0 \le \alpha^{j}_{DG_i} P^{max}_{i} \le P^{max}_{i} \\ 0 \le \alpha^{j}_{FC} P^{max}_{FC} \le P^{max}_{FC} \\ -P^{max,c}_{BESS} \le P_{FC_j} + \sum\limits_{i=1}^{n} P_{i,j} - P_{load_j} \le P^{max,d}_{BESS} \\ SoC^{min} \le SoC_j \le SoC^{max} \\ SoC_0 = SoC_T \\ m_{H_2} \le H^{on-board}_{2} \end{cases} \tag{33}$$

Eq. (33) presents a constrained minimum problem that can be solved with a numerical solver. There are several solvers available for constrained optimization problems, such as NLopt [37], SciPy's optimize library [38], Gurobi [39], COIN-OR [40], and MATLAB Optimization Toolbox [41], which support a wide range of algorithms including gradient-based methods, evolutionary algorithms, and metaheuristic approaches. These libraries are widely used and cross-platform, making the choice of solver independent from the methodology itself. In the present paper the MATLAB Optimization Toolbox was used to handle linear and nonlinear equality and inequality constraints. In particular, the general-purpose nonlinear programming solver "fmincon" allows solving a minimum problem with user-defined loss function, linear, and nonlinear constraints. To avoid being trapped in local minima, a multi-start approach was used, randomly initializing the starting point of the algorithm to increase the chances of converging to the global minimum.

5. Case study

The case study vessel used to apply the described optimization strategy is a ferry boat whose main data are presented in Table 3. The power system includes 3×400 kW DG, a 1 MWh battery pack, and 10×34 kW fuel cell modules for a total power of 340 kW, providing power to two Electric Propulsion Motors moving two fixed pitch propellers, and the hotel load. The battery pack allows zero-emission navigation at low speed (e.g., within Marine Protected Areas) and in port, as well as the smart loading of the DG to reduce fuel consumption. A schematic representation of the propulsion system configuration is given in Fig. 3.

Table 3
General and propulsion system specifications of the case study ferry.

Length between perpendiculars	28.73 m
Breadth	7.02 m
Depth	2.60 m
Draft	1.22 m
Displacement	120 t
Cruise speed	18 Kn
Low speed	13 Kn
Passenger	516
DG power	400 kW
Number of DG	3
Battery capacity	1 MWh
Fuel cell power	340 kW
Hydrogen on-board	500 kg

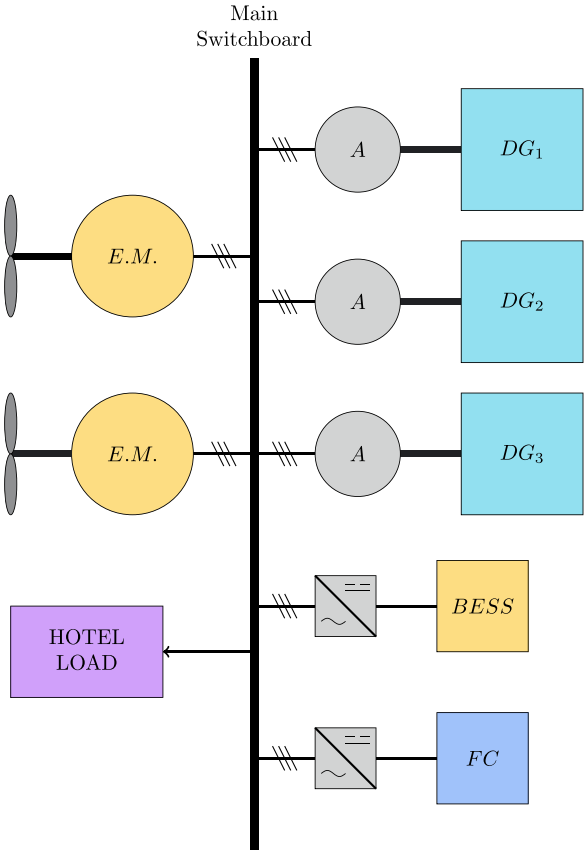

Fig. 3. Propulsion system configuration scheme.

The ship operates in the eastern Ligurian Riviera, in the La Spezia area shown in Fig. 5. Specifically, the route connects La Spezia and Levanto ports through the "Cinque Terre" Marine Protected Area. The ship navigates from La Spezia to Portovenere at a regular cruising speed in the first route leg. After a brief stop to pick up and drop off passengers, the ferry proceeds to the port of Riomaggiore. In this leg, the ship keeps its cruising speed until it enters the "Cinque Terre" Marine Protected Area, where the speed is reduced to 13 Kn. The other intermediate stops within the marine protected area include Manarola, Vernazza, and Monterosso.

The ferry here maintains a constant speed of 13 Kn, with short breaks between segments for passengers to embark and disembark. The

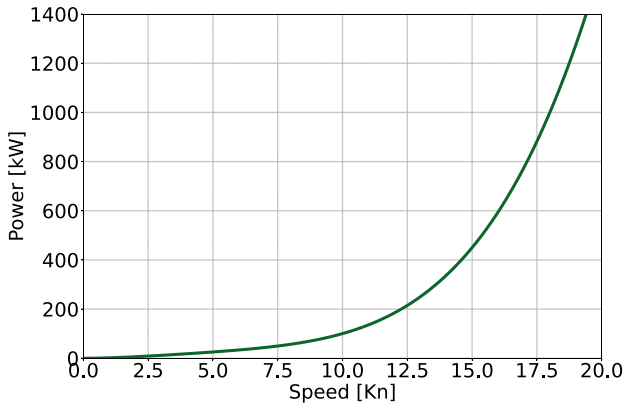

Fig. 4. Propulsive power curve in function of ship's speed.

Table 4
Details of the mission profile.

Route leg	Distance	Speed	Duration
La Spezia - Portovenere	3.9 nm	18 Kn	13 min
Dock stop	–	–	*20* min
Portovenere - Marine protected area entrance	4.25 nm	18 Kn	14 min
Marine protected area entrance - Riomaggiore	2 nm	13 Kn	10 min
Dock stop	–	–	*20* min
Riomaggiore - Manarola	0.8 nm	13 Kn	4 min
Dock stop	–	–	*20* min
Manarola - Vernazza	2.7 nm	13 Kn	13 min
Dock stop	–	–	*20* min
Vernazza - Monterosso	1.5 nm	13 Kn	7 min
Dock stop	–	–	*20* min
Monterosso - Marine protected area exit	3.2 nm	13 Kn	15 min
Marine protected area exit - Levanto	1.6 nm	18 Kn	5 min
Dock stop	–	–	*80* min
Levanto - Marine protected area entrance	1.6 nm	18 Kn	5 min
Marine protected area entrance - Monterosso	3.2 nm	13 Kn	15 min
Dock stop	–	–	*20* min
Monterosso - Vernazza	1.5 nm	13 Kn	7 min
Dock stop	–	–	*20* min
Vernazza - Manarola	2.7 nm	13 Kn	13 min
Dock stop	–	–	*20* min
Manarola - Riomaggiore	0.8 nm	13 Kn	4 min
Dock stop	–	–	*20* min
Riomaggiore - Marine protected area exit	2 nm	13 Kn	10 min
Marine protected area exit - Portovenere	4.25 nm	18 Kn	14 min
Dock stop	–	–	*20* min
Portovenere - La Spezia	3.9 nm	18 Kn	13 min
Dock stop	–	–	*80* min

mission profile of the vessel is summarized in Table 4. The propulsive power in function of the ferry speed is shown in Fig. 4, while the hotel load is assumed constant and equal to 50 kW. Fig. 6 shows the corresponding required power for the mission.

The algorithm was tested in three different propulsion system cases, obtained by combining the power sources available on-board. In particular, the following cases have been considered and compared:

- DG:This case uses only the DG on-board;
- $DG/BESS$: in this case, both DG and the $BESS$ are used.
- $DG/BESS/FC$: this case considers the full stack of power sources available on-board, i.e., the generators, the $BESS$, and the fuel cell. This case is split into five sub-cases depending on the hydrogen production technology (Table 2):
  - $DG/BESS/FC/K$: "gray" hydrogen, produced by steam methane reforming;
  - $DG/BESS/FC/B56$: "blue" hydrogen with 56% carbon capture and storage;
  - $DG/BESS/FC/B90$: "blue" hydrogen with 90% carbon capture and storage;
  - $DG/BESS/FC/T$: "turquoise" hydrogen from methane pyrolysis;
  - $DG/BESS/FC/G$: "green" hydrogen from the Italian production toolchain (mostly nonrenewable energy);
  - $DG/BESS/FC/G+$: "green" hydrogen from the Norwegian production toolchain (mostly renewable energy).

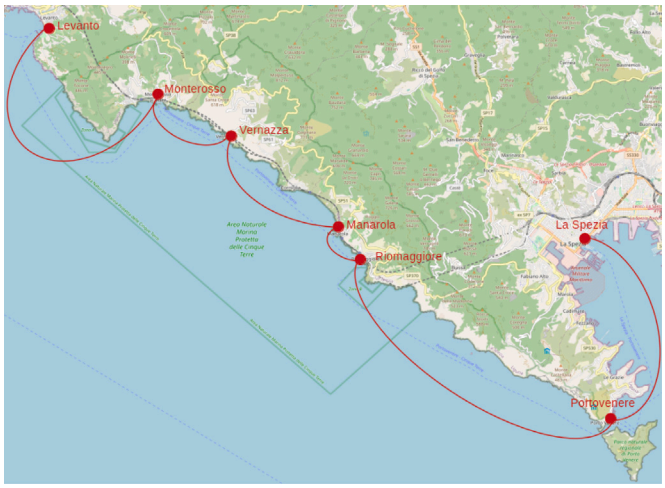

Fig. 5. The "Cinque Terre" Marine Protected Area.

6. Results

The algorithm was tested in each case listed in Section 5. This section presents and discusses the obtained results. In particular, for each case, the following results are provided:

- A graphical representation of the power split on-board, showing how the load is shared over time;
- A graphical representation of the State-of-Charge over time, if the considered case includes the $BESS$.

Moreover, fuel and hydrogen consumption time histories are compared for each configuration. Eventually, the annual fuel and hydrogen consumption and equivalent CO_2 emissions are compared for the considered cases. The following subsections discuss every case in detail.

6.1. Case DG

In case DG, minimizing the equivalent CO_2 emissions corresponds to minimizing the fuel mass flow rate at every t_j. Fig. 7 shows the power split among the DG. This case will be used later as a reference to evaluate whether the use of hybrid technologies can reduce the ferry's environmental impact.

6.2. Case DG/BESS

Case DG/BESS includes DG and $BESS$ on-board. Fig. 8(a) presents the power split among the components. Fig. 8(b) shows the battery State-of-Charge during the mission. The diesel generators charge the batteries during the more extended port stop to use the stored energy to cruise with zero emissions in other low-speed phases of the mission. As opposed to case DG, which uses diesel generators at low load and low efficiency, case DG/BESS uses the battery as a reservoir of energy that is generated at high efficiency when the power demand is low, to use when the power demand is high or to switch off the DG completely.

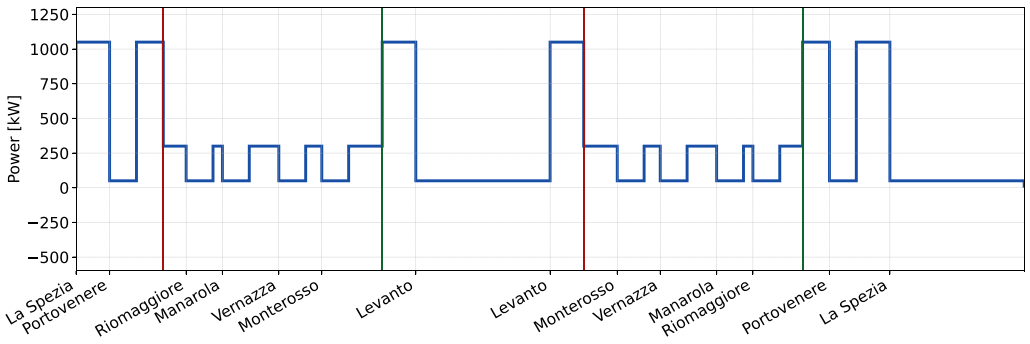

Fig. 6. Required power profile over the mission.

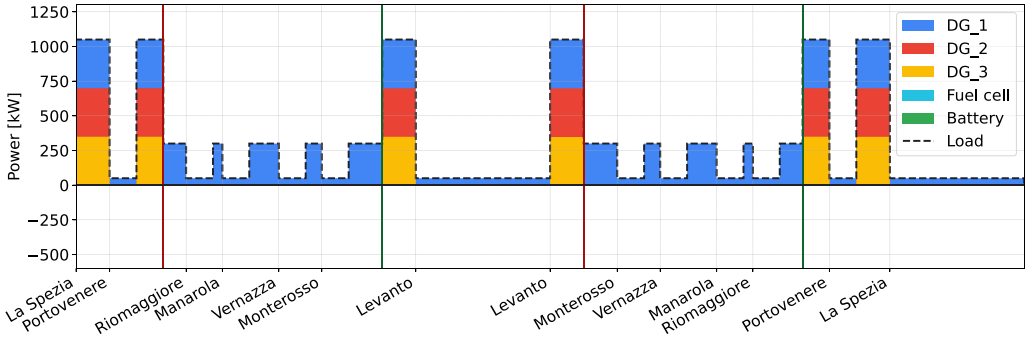

Fig. 7. Case DG - Power split.

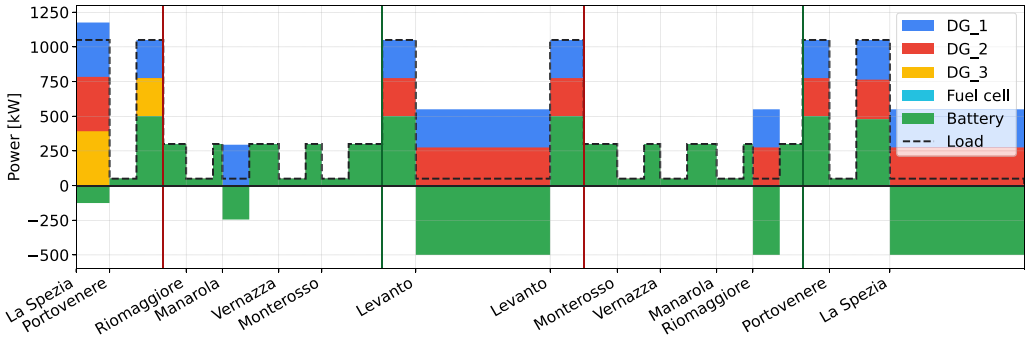

a: Power split

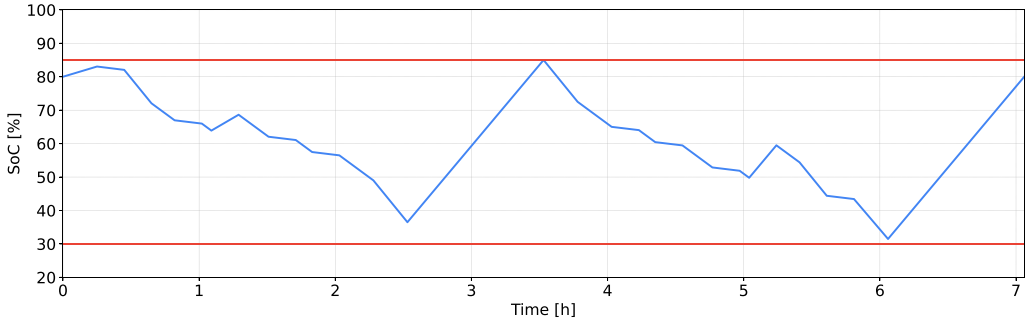

b: State-of-Charge

Fig. 8. Case $DG/BESS$.

6.3. Case DG/BESS/FC

In this case, all the components can generate power. Different results are obtained depending on the hydrogen production technology. In particular, when the emission factor is high, using the fuel cell is penalizing even compared with traditional diesel internal combustion engines. If hydrogen's emission factor is comparable with diesel fuel, the fuel cells can still be effective at low loads because of the higher efficiency, but from a particular emission factor value onward,

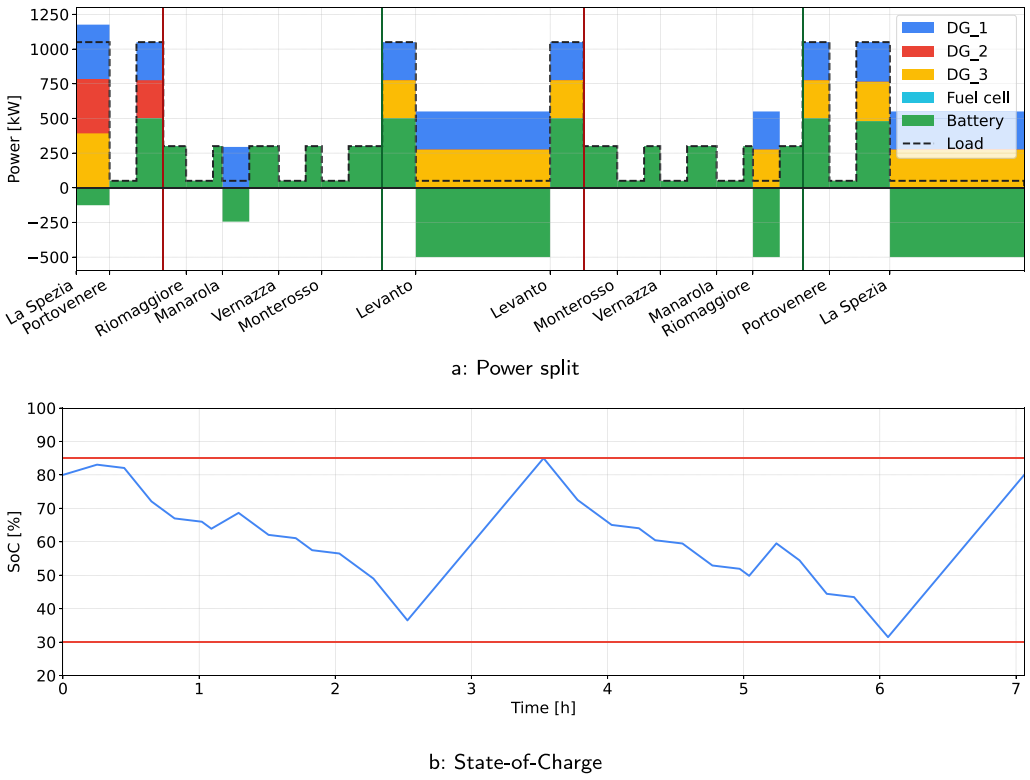

Fig. 9. Case DG/BESS/FC/B56.

it becomes counterproductive. The threshold value for this mission has been determined empirically to 6.6 $CO_{2\,eq}$/kg H_2, meaning that "gray", "turquoise", and "blue" hydrogen with 56% CCS, as well as "green" hydrogen produced with nonrenewable sources (e.g., Italy), do not provide benefits to reducing environmental impact. The results have been collected under the label DG/BESS/FC/K,B56,T,G, showing similar results to case DG/BESS. Fig. 9(a) presents the power split time history, while Fig. 9(b) shows the battery state of charge.

In case DG/BESS/FC/B90, "Blue" hydrogen with 90% carbon capture and storage improves the results. Fig. 10(a) shows that only fuel cells and batteries are used to power the unit within the marine protected area, where power demand is not very high. The dock stop in Riomaggiore is an exception since a DG is used at optimal load to recharge the battery, and the fuel cell is used to achieve the required power. Similar behavior is registered during the long stops in La Spezia and Levanto. In the navigation phase between La Spezia and Portovenere, where the load power is high, the three generators plus the fuel cell meet the load power and recharge the battery to 85% (Fig. 10(b)).

The best result is achievable if hydrogen is produced by water electrolysis mainly using renewable sources (case DG/BESS/FC/G+), such as in the case of Norway [19]. In case DG/BESS/FC/G+, the algorithm makes extensive use of the fuel cells, even to recharge the batteries when the power demand is low (Figs. 11(a), 11(b)), to maximize the amount of zero-emission power available in high power demand phases, to minimize the use of DG to the particular conditions when $BESS$ and fuel cells cannot meet the required power.

6.4. Comparison

Figs. 12 and 13 compare the consumption and emissions of the considered propulsive configurations. In particular, Figs. 12(a) and 12(b) compare the fuel and the hydrogen consumption over the mission, while Figs. 13(a), 13(b), 13(c) compare the annual fuel consumption, the annual hydrogen consumption, and the equivalent CO_2 emission, for the different cases, assuming the ferry performs two daily missions for 310 working days per year. Notice that case DG produces the most significant greenhouse gas emissions, as expected. By integrating a battery pack with the propulsion system, the emissions, and fuel consumption can be significantly reduced. In case DG/BESS/FC, where fuel cells are integrated into the system, the results largely depend on the hydrogen production technology. In particular, only "blue" hydrogen with 90% CCS (case DG/BESS/FC/B90) and "green" hydrogen from renewable sources (case DG/BESS/FC/G+) benefit the ferry's environmental impact, largely reducing the yearly equivalent CO_2 emissions.

7. Conclusion

The paper presented an optimization strategy aimed at determining the optimal operating strategy to minimize the environmental impact of a hybrid marine propulsion system. Specifically, a static performance-based lumped-element modeling approach to the propulsion system was described and used to set up an optimization problem. The proposed strategy has been applied to a case study regarding a small ferry boat operating in a marine protected area. The case study featured and compared different system configurations, including diesel generators only, a hybrid diesel-$BESS$ configuration, and the fully featured hybrid configuration, including diesel generators, $BESS$, and hydrogen-powered fuel cells. The comparison included different hydrogen production technologies.

The results showed that hybrid systems with $BESS$ lead to a 27%$CO_{2\,eq}$ emission reduction. Hydrogen's effectiveness mainly depends on the technology with which it is produced. Since the leading hydrogen production technology is "gray", its use as an energy carrier is not cost-effective from the point of view of environmental impact. "Green" hydrogen produced with $PEMEL$ technology proves effective only if it is produced using renewable sources (as in Norway, DG/BESS/FC/G+), leading to a 73% reduction in emissions compared to the case DG. Using blue hydrogen with 90% CCS

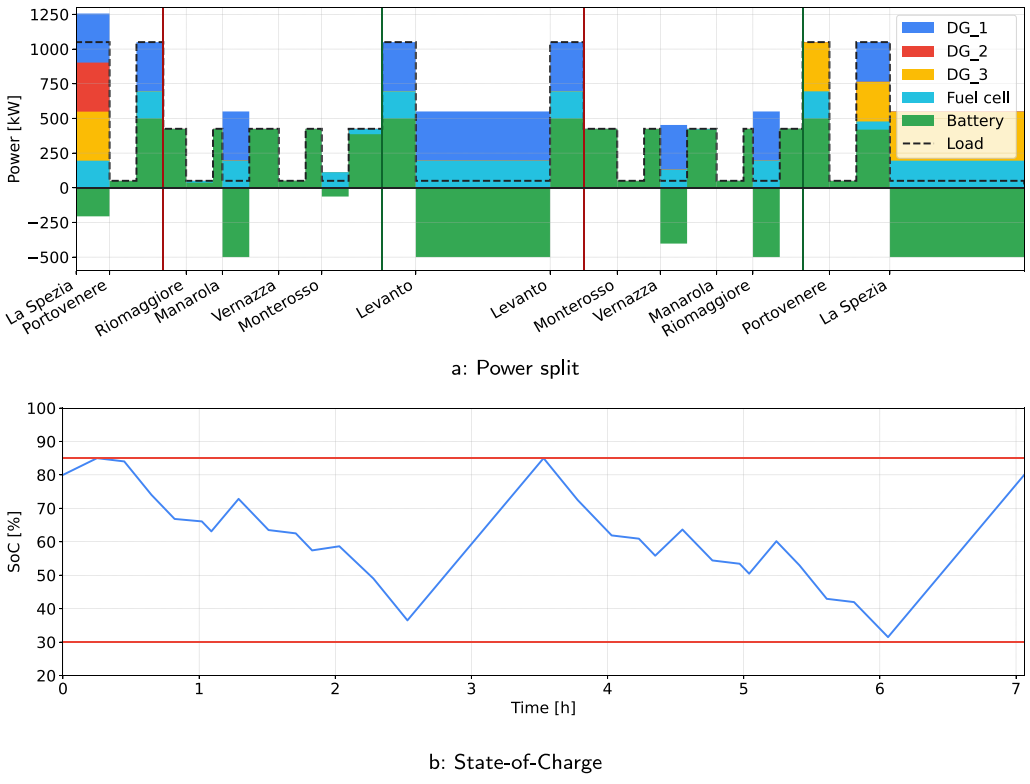

Fig. 10. Case DG/BESS/FC/B90.

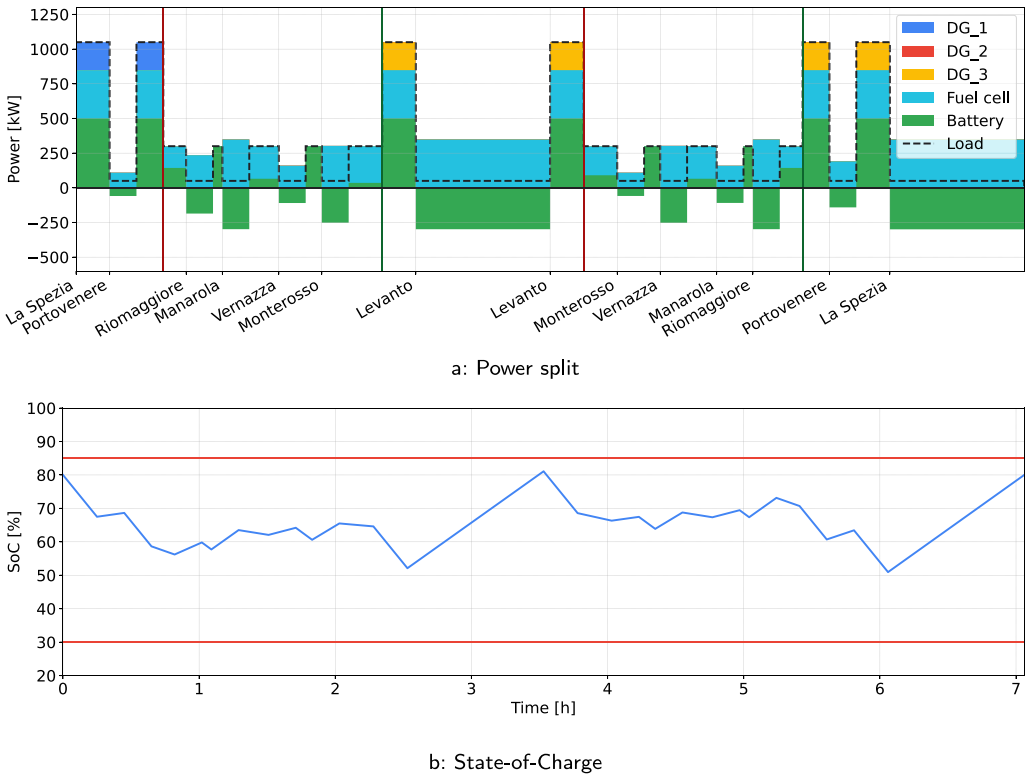

Fig. 11. Case DG/BESS/FC/G+.

(DG/BESS/FC/B90) provides better results than case DG, yet it provides an emission reduction of only $12t/y$ compared to case DG/BESS.

Eventually, some open questions can be discussed. First, the rationale for using different energy resources is based solely on minimizing emissions on the entire trip. A multi-objective approach could allow, for example, to evaluate the trade-off between minimizing overall emissions and minimizing emissions in some specific parts of the mission, such as the marine protected area. Moreover, the model could be

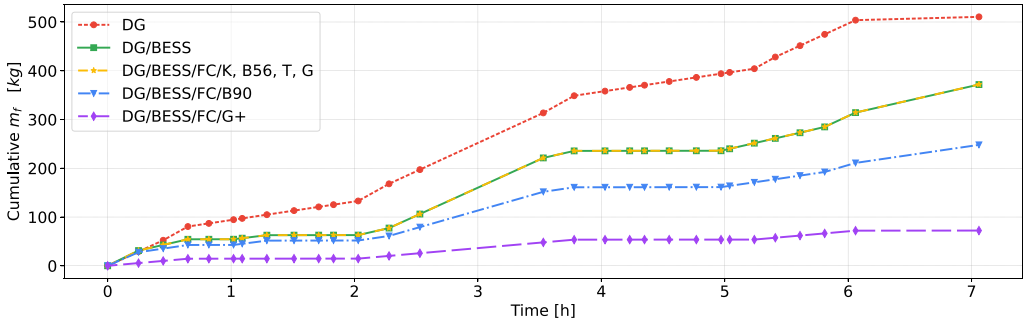

a: Fuel consumption

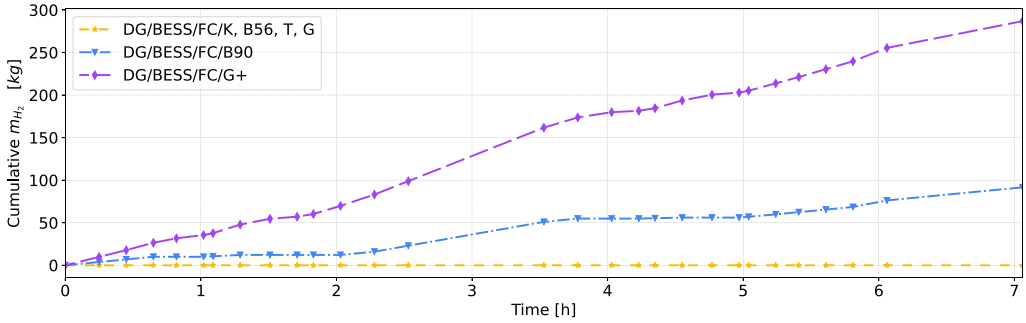

b: H_2 consumption

Fig. 12. Comparison of fuel and H_2 consumption over the mission.

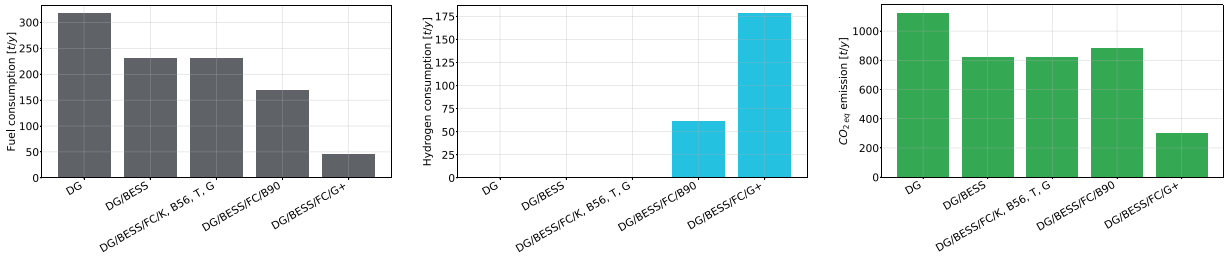

a: Fuel consumption per year b: H_2 consumption per year c: $CO_{2\,eq}$ emission per year

Fig. 13. Comparison of the different considered cases over a year of operation, assuming two missions per day and 310 working days per year.

extended by considering alternative fuels, for instance, methanol, and the supply chain of resources from shore, for example, by including the availability of hydrogen for refueling at some shore stations or the presence of electrified docks that could provide power to batteries during stopovers at the cost of emissions from the national power grid. In addition, the presented strategy allows for the determination of the optimal power split known from the power demand time history. It thus allows comparison of the performance of different plant configurations applied to the same mission profile. By structuring this step in a systematic and generalized manner, the proposed strategy can be integrated into an optimization loop capable of determining the optimal plant configuration to deal with one or more typical mission profiles. Eventually, it would be appropriate to investigate the potential of the proposed strategy coupled with a predictive power demand methodology, and to finally evaluate its benefits within as a part of a real-time optimal power management and control system for a hybrid power generation plant.

CRediT authorship contribution statement

Luca Maloberti: Writing – original draft, Visualization, Software, Methodology, Investigation, Formal analysis, Conceptualization. **Raphael Zaccone:** Writing – review & editing, Validation, Supervision, Software, Methodology, Conceptualization.

Declaration of competing interest

The authors declare that they have no known competing financial interests or personal relationships that could have appeared to influence the work reported in this paper.

Data availability

No data was used for the research described in the article.

References

[1] Bouman EA, Lindstad E, Rialland AI, Strømman AH. State-of-the-art technologies, measures, and potential for reducing ghg emissions from shipping–a review. Transp Res D: Transp Environ 2017;52:408–21.

[2] Jägerbrand AK, Brutemark A, Sveden JB, Gren M. A review on the environmental impacts of shipping on aquatic and nearshore ecosystems. Sci Total Environ 2019;695:133637.

[3] Cabezas-Basurko O, Mesbahi E, Moloney S. Methodology for sustainability analysis of ships. Ships Offshore Struct 2008;3:1–11.

[4] M.O. T.I I. Greenhouse gas study. Executive summary and final report, London; 2014.

[5] Livanos GA, Theotokatos G, Pagonis DN. Techno-economic investigation of alternative propulsion plants for ferries and roro ships. Energy Convers Manage 2014;79:640–51.

[6] Nielsen RF, Haglind F, Larsen U. Design and modeling of an advanced marine machinery system including waste heat recovery and removal of sulphur oxides. Energy Convers Manage 2014;85:687–93.

[7] Tadros M, Ventura M, Soares CG. Review of current regulations, available technologies, and future trends in the green shipping industry. Ocean Eng 2023;280:114670.

[8] Maloberti L, Zaccone R, Gualeni P, Mazzucchelli P. A zero-emission ferry for inland waterways. In: Technology and science for the ships of the future. IOS Press; 2022, p. 162–9.

[9] Han J, Charpentier JF, Tang T. State of the art of fuel cells for ship applications. In: 2012 IEEE international symposium on industrial electronics. IEEE; 2012, p. 1456–61.

[10] Lindstad E, Lagemann B, Rialland A, Gamlem GM, Valland A. Reduction of maritime ghg emissions and the potential role of e-fuels. Transp Res D: Transp Environ 2021;101:103075.

[11] Jimenez VJ, Kim H, Munim ZH. A review of ship energy efficiency research and directions towards emission reduction in the maritime industry. J Clean Prod 2022;132888.

[12] Inal OB, Charpentier JF, Deniz C. Hybrid power and propulsion systems for ships: Current status and future challenges. Renew Sustain Energy Rev 2022;156:111965.

[13] Mofor L, Nuttall P, Newell A. Renewable energy options for shipping-technology brief. IRENA Innovation and Technology Center; 2014.

[14] Carlton J, Aldwinkle J, Anderson J, et al. Future ship powering options: exploring alternative methods of ship propulsion. London: Royal Academy of Engineering; 2013.

[15] Mallouppas G, Yfantis EA. Decarbonization in shipping industry: A review of research, technology development, and innovation proposals. J Mar Sci Eng 2021;9:415.

[16] Belvisi D, Zaccone R, Figari M, Simone S, Spanghero B. Bess-based hybrid propulsion: An application to a front line naval vessel preliminary design. In: Progress in marine science and technology - proceedings of the 20th international conference on ship and maritime research, NAV 2022. 2022, p. 154–61. http://dx.doi.org/10.3233/PMST220020.

[17] Domenech Rd'Amore, Leo TJ, Pollet BG. Bulk power transmission at sea: Life cycle cost comparison of electricity and hydrogen as energy vectors. Appl Energy 2021;288:116625.

[18] Benet Á, Villalba-Herreros A, Domenech Rd'Amore, Leo TJ. Knowledge gaps in fuel cell-based maritime hybrid power plants and alternative fuels. J Power Sources 2022;548:232066.

[19] Hermesmann M, Müller T. Green, turquoise, blue, or grey? environmentally friendly hydrogen production in transforming energy systems. Prog Energy Combust Sci 2022;90:100996.

[20] Zaccone R, Campora U, Martelli M. Optimisation of a diesel-electric ship propulsion and power generation system using a genetic algorithm. J Mar Sci Eng 2021;9:587.

[21] D'Agostino F, Gallo M, Saviozzi M, Silvestro F. A security-constrained optimal power management algorithm for shipboard microgrids with battery energy storage system. 2023, arXiv preprint arXiv:2304.03621.

[22] Al-Falahi MD, Nimma KS, Jayasinghe SD, Enshaei H, Guerrero JM. Power management optimization of hybrid power systems in electric ferries. Energy Convers Manage 2018;172:50–66.

[23] Kanellos F. Optimal power management with ghg emissions limitation in all-electric ship power systems comprising energy storage systems. IEEE Trans Power Syst 2013;29:330–9.

[24] Gallo M, Kaza D, D'Agostino F, Cavo M, Zaccone R, Silvestro F. Power plant design for all-electric ships considering the assessment of carbon intensity indicator. Energy 2023;283:129091.

[25] Heywood JB. Internal combustion engine fundamentals. McGraw-Hill Education; 2018.

[26] Ashok B, Nanthagopal K, Vignesh DS. Calophyllum inophyllum methyl ester biodiesel blend as an alternate fuel for diesel engine applications. Alex Eng J 2018;57:1239–47.

[27] Ghimire P, Zadeh M, Thorstensen J, Pedersen E. Data-driven efficiency modeling and analysis of all-electric ship powertrain: A comparison of power system architectures. IEEE Trans Transp Electrif 2021;8:1930–43.

[28] Meng J, Luo G, Ricco M, Swierczynski M, Stroe DI, Teodorescu R. Overview of lithium-ion battery modeling methods for state-of-charge estimation in electrical vehicles. Appl Sci 2018;8:659.

[29] Zaccone R, Figari M, Martelli M. A simulation based tool to assess the propulsion performance of modern conventional submarines. In: 2022 international symposium on power electronics, electrical drives, automation and motion. SPEEDAM, IEEE; 2022, p. 628–33.

[30] Saadi A, Becherif M, Aboubou A, Ayad M. Comparison of proton exchange membrane fuel cell static models. Renew Energy 2013;56:64–71.

[31] Fan L, Li C, Boshnakov K. Performance comparison of three different controllers of proton exchange membrane fuel cell. Open Fuels Energy Sci J 2015;8.

[32] Chakraborty UK. Reversible and irreversible potentials and an inaccuracy in popular models in the fuel cell literature. Energies 2018;11(1851).

[33] Santarelli MG, Torchio MF, Cochis P. Parameters estimation of a pem fuel cell polarization curve and analysis of their behavior with temperature. J Power Sources 2006;159:824–35.

[34] Jun P, Gillenwater M, Barbour W. Co2, ch4, and n2o emissions from transportation–water-borne navigation. In: Good practice guidance and uncertainty management in national greenhouse gas inventories. Paris, France: intergovernmental panel on climate change; 2000, p. 71–92.

[35] Woodcock N. Houghton, jt, meira filho, lg, callander, ba, harris, n., kattenberg, a. & maskell, k.(eds) 1996. climate change 1995. the science of climate change. contribution of working group 1 to the second assessment report of the intergovernmental panel on climate change. xii+ 572 pp. cambridge, new york, port chester, melbourne, sydney: cambridge university press for the intergovernmental panel on climate change. price£ 65.00, us 34.95 (paperback). isbn 0 521 56433 6 0 521 56436 0 (pb). Geol Mag 1997;134:269–81.

[36] Yousefi M, Damghani AMahdavi, Khoramivafa M. Comparison greenhouse gas (ghg) emissions and global warming potential (gwp) effect of energy use in different wheat agroecosystems in iran. Environ Sci Pollut Res 2016;23:7390–7.

[37] Johnson SG. The NLopt nonlinear-optimization package. 2007, https://github.com/stevengj/nlopt.

[38] Virtanen P, Gommers R, Oliphant T, Haberland M, Reddy T, Cournapeau D, Burovski E, Peterson P, Weckesser W, SciPy JB. 1.0: Fundamental algorithms for scientific computing in python. 2020, p. 17. http://dx.doi.org/10.1038/s41592-019-0686-2, 261–272.

[39] Achterberg T, Bixby RE, Gu Z, Rothberg E, Weninger D. Presolve reductions in mixed integer programming. INFORMS J Comput 2020;32:473–506.

[40] Lougee-Heimer R. The common optimization interface for operations research: Promoting open-source software in the operations research community. IBM J Res Dev 2003;47:57–66.

[41] The MathWorks Inc. Optimization toolbox version: 9.4 r2022b. 2022, URL https://www.mathworks.com.